Clinical Science (2023) **137** 367–383
https://doi.org/10.1042/CS20220876

PORTLAND PRESS

Research Article

Interferon regulatory factor 1 (IRF1) inhibits lung endothelial regeneration following inflammation-induced acute lung injury

Xiaorui Chen[1], Di Qi[1], Shulei Fan[1], Yirui He[2], Hekun Jing[1] and Daoxin Wang[1]

[1]Department of Respiratory and Critical Care Medicine, the Second Affiliated Hospital, Chongqing Medical University, Chongqing, China; [2]Department of Endocrinology, the Second Affiliated Hospital, Chongqing Medical University, Chongqing, China

Correspondence: Xiaorui Chen (cherrycxr123456@qq.com) or Daoxin Wang (wangdaoxin@hospital.cqmu.edu.cn)

Background: Acute respiratory distress syndrome (ARDS) is a respiratory condition caused by severe endothelial barrier dysfunction within the lung. In ARDS, excessive inflammation, tissue edema, and immune cell influx prevents endothelial cell regeneration that is crucial in repairing the endothelial barrier. However, little is known about the molecular mechanism that underpin endothelial cell regeneration in ARDS.
Methods: R-based bioinformatics tools were used to analyze microarray-derived transcription profiles in human lung microvascular endothelial cells (HLMVECs) subjected to non-treatment or lipopolysaccharide (LPS) exposure. We generated endothelial cell-specific interferon regulatory factor 1 (*Irf1*) knockout ($Irf1^{EC-/-}$) and $Irf1^{fl/fl}$ control mice for use in an endotoxemic murine model of acute lung injury (ALI). *In vitro* studies (qPCR, immunoblotting, and ChIP-qPCR) were conducted in mouse lung endothelial cells (MLECs) and HLMVECs. Dual-luciferase promoter reporter assays were performed in HLMVECs.
Results: Bioinformatics analyses identified *IRF1* as a key up-regulated gene in HLMVECs post-LPS exposure. Endothelial-specific knockout of *Irf1* in ALI mice resulted in enhanced regeneration of lung endothelium, while liposomal delivery of endothelial-specific *Irf1* to wild-type ALI mice inhibited lung endothelial regeneration in a leukemia inhibitory factor (Lif)-dependent manner. Mechanistically, we demonstrated that LPS-induced $Stat1^{Ser727}$ phosphorylation promotes Irf1 transactivation, resulting in downstream up-regulation of Lif that inhibits endothelial cell proliferation.
Conclusions: These results demonstrate the existence of a p-$Stat1^{Ser727}$-Irf1-Lif axis that inhibits lung endothelial cell regeneration post-LPS injury. Thus, direct inhibition of IRF1 or LIF may be a promising strategy for enhancing endothelial cell regeneration and improving clinical outcomes in ARDS patients.

Introduction

Acute respiratory distress syndrome (ARDS) is a respiratory condition caused by severe endothelial barrier dysfunction within the lung [1]. Patients with ARDS typically present with acute dyspnea, hypoxemia, pulmonary edema, tachycardia, systemic inflammation, and, in severe cases, multiple organ dysfunction [1]. As the underlying molecular mechanism(s) underlying endothelial dysfunction are not fully understood, effective therapies are yet to be discovered [1]. Instead, ARDS patients often require ventilator and fluid/electrolyte support, and the mortality rate for ARDS patients remains extremely high. In one multi-center prospective cohort of 3022 ARDS patients, mortality rates among mild, moderate, and severe ARDS patients were 35%, 40%, and 46%, respectively [2].

Received: 14 December 2022
Revised: 27 February 2023
Accepted: 01 March 2023

Accepted Manuscript online: 01 March 2023
Version of Record published: 09 March 2023

Clinical Science (2023) **137** 367–383
https://doi.org/10.1042/CS20220876

Endothelial barrier dysfunction results from endothelial cell injury or death [3]. Regeneration of endothelial cells is, therefore, crucial in order to repair the barrier [3]. During the pathogenesis of ARDS, excessive inflammation, tissue edema, and an influx of immune cells often prevents endothelial cell regeneration [3]. Consequently, recent studies have attempted to use stem cell or endothelial progenitor cells to restore endothelial homeostasis following injury [4,5]. Due to the challenges of using stem cells clinically [6,7], an alternate approach has been to reactivate the intrinsic repair mechanisms that underpin endothelial cell regeneration [3]. However, to date, little is known about the molecular mechanism(s) that underpin endothelial cell regeneration in ARDS.

Type I interferons (IFNs) are pleiotropic cytokines involved in innate immunity [8]. Due to their involvement in inflammatory processes, IFN pathways could also play a role in endothelial damage and/or regeneration [8]. Studies in human umbilical vein endothelial cells (HUVECs) demonstrated that IFN-β can initiate cell cycle arrest and therefore inhibit proliferation [9,10]. Notably, IFN-β profoundly affects endothelial transcriptional programming by stimulating Tyr701 phosphorylation and nuclear translocation of the transcription factor STAT1 [11], forming the potent IFN-β/p-STAT1^{Tyr701} signaling axis. Moreover, a genome-wide integranomics study identified the IFN-β/p-STAT1^{Tyr701} signaling effector interferon regulatory factor 1 (IRF1) as a key transcription factor that coordinates endothelial gene expression under pro-inflammatory stimuli [12]. Notably, transcriptomic analysis of IRF1-transduced fibroblasts shows that IRF1-bound targets in IFN-treated cells are associated with apoptosis-related gene transactivation [13]. In slight contrast with IFN-β, lipopolysaccharide (LPS) activates p38 mitogen-activated protein kinase (p38 MAPK), which stimulates Ser727 phosphorylation (but not Tyr701 phosphorylation) of STAT1 in endothelial cells [14]. This LPS-induced Ser727 phosphorylation of STAT1 enhances STAT1's DNA binding activity [14], suggesting that LPS acts independently of IFN-β in stimulating STAT1 signaling activity in endothelial cells via STAT1^{Ser727} phosphorylation.

As this evidence suggests that the p-STAT1/IRF1 axis may play an anti-proliferative/pro-apoptotic role in endothelial cells under pro-inflammatory conditions, we hypothesized that LPS-induced endothelial injury would enhance endothelial STAT1^{Ser727} phosphorylation and downstream IRF1 transactivation, thereby inhibiting lung endothelial regeneration. Using a LPS-induced endotoxemic murine model of acute lung injury (ALI), we demonstrate that endothelial IRF1 plays an inhibitory role in regeneration of the lung endothelium. Specifically, we discovered that endothelial integrity is compromised by p-STAT1^{Ser727}-mediated IRF1 transactivation and downstream leukemia inhibitory factor (LIF)-mediated endothelial proliferative retardation.

Materials and methods

Bioinformatics analysis

Bioinformatics analysis was performed on Harry et al.'s published GEO dataset (GSE5883), in which cultured human lung microvascular endothelial cells (HLMVECs) were left untreated (control, Ctrl) or exposed to LPS (10 ng) for four hours ($n = 4$ biological replicates per group); isolated, amplified RNA therefrom was subjected to Affymetrix HG U133plus2 gene array analysis. The four-hour timepoint was selected for analysis, as it is the earliest timepoint reported in the literature at which LPS significantly enhances human endothelial cell death and permeability *in vitro* [15,16].

The weighted correlation network analysis (WGCNA)-based modular analysis on the raw GSE5883 microarray data comparing LPS-exposed HLMVECs against Ctrl HLMVECs was performed using the Cemitool package. The module annotation was performed with Human Reactome v7.1. The interaction network and Gene Set Enrichment Analysis (GSEA) algorithms were available within the Cemitool package. The following parameters were employed: filter = TRUE, filter_pval = 0.1, apply_vst = FALSE, n_genes = FALSE, eps = 0.1, cor_method = 'pearson', cor_function = 'cor', network_type = 'unsigned', tom_type = 'signed', set_beta = NULL, force_beta = TRUE, merge_similar = TRUE, rank_method = 'mean', ora_pval = 0.05, and gsea_scale = TRUE.

For differentially expressed gene (DEG) analysis, the raw GSE5883 microarray data was first subjected to median-based filtration and quantile normalization. DEGs from LPS-exposed HLMVECs versus Ctrl HLMVECs were then identified using the limmapackage moderated *t*-test with an adjusted *P*-value threshold of $P<0.05$ for multiple testing. A volcano plot was used to illustrate DEGs by module membership with statistical significance versus $\log_2$fold-change ($\log_2$FC) on the *y*- and *x*-axes, respectively; profoundly dysregulated DEGs were defined by a $|\log_2 FC|>1.0$ threshold. The heatmap of the most up-regulated M2 genes was generated in R via the heatmap.2 function from the gplots package, using the 'scale' = 'row' switch to Z-score standardize the rows. Gene expression is shown in red and green, with red corresponding to low expression and green corresponding to high expression.

To identify which of the target gene(s) showed the strongest relationships with endothelial regeneration in the existing literature, a Web-based term association analysis was performed by searching Google Scholar with the search

Clinical Science (2023) **137** 367–383
https://doi.org/10.1042/CS20220876

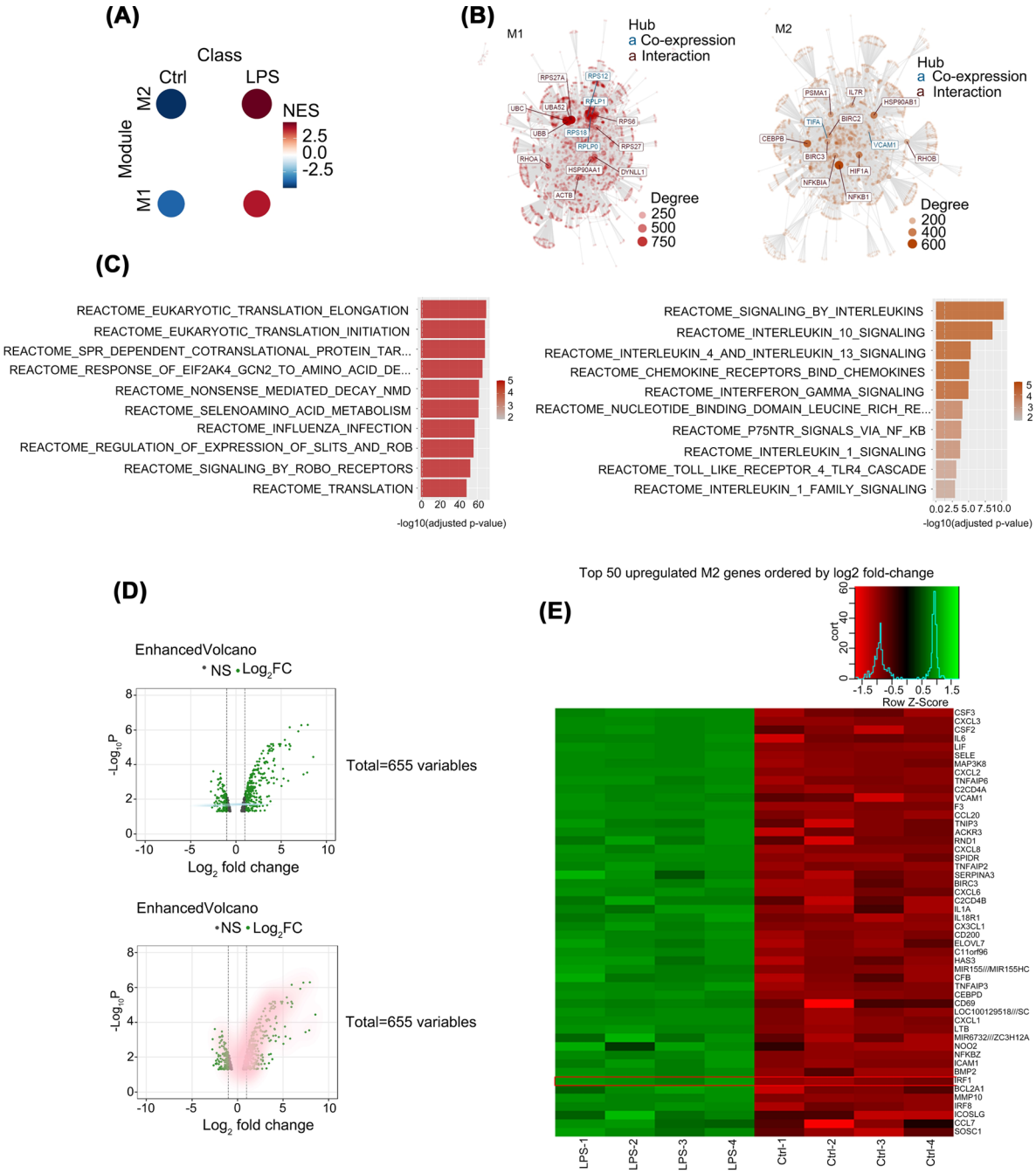

Figure 1. R-based bioinformatics analysis identifies Irf1 as a key up-regulated gene in LPS-exposed murine lung endothelial cells

R-based bioinformatics analysis of published microarray data (GEO acc no. GSE5883) in which cultured human lung microvascular endothelial cells (HLMVECs) were left untreated (Ctrl) or exposed to LPS (10 ng) for 4 h (n = 4 biological replicates per group). (**A**) Gene set enrichment analysis (GSEA)-based identification of two discreet gene co-expression modules associated with LPS exposure: M1 and M2. Red coloring denotes a positive NES score, while blue coloring denotes a negative NES score. (**B**) Network plots for the two gene co-expression modules M1 and M2. (**C**) Reactome enrichment analysis for the two gene co-expression modules M1 and M2. The color saturation denotes the prediction confidence. (**D**) Volcano plots of differentially expressed genes (DEGs) with staining for M1 module membership (blue, top panel) or M2 module membership (pink, bottom panel). (**E**) Heatmap of the top 50 M2 module up-regulated DEGs ordered by descending log2 fold-change. Up-regulation is denoted by green coloring, while down-regulation is denoted by red coloring. *IRF1* is marked by a red rectangle.

Clinical Science (2023) **137** 367–383
https://doi.org/10.1042/CS20220876

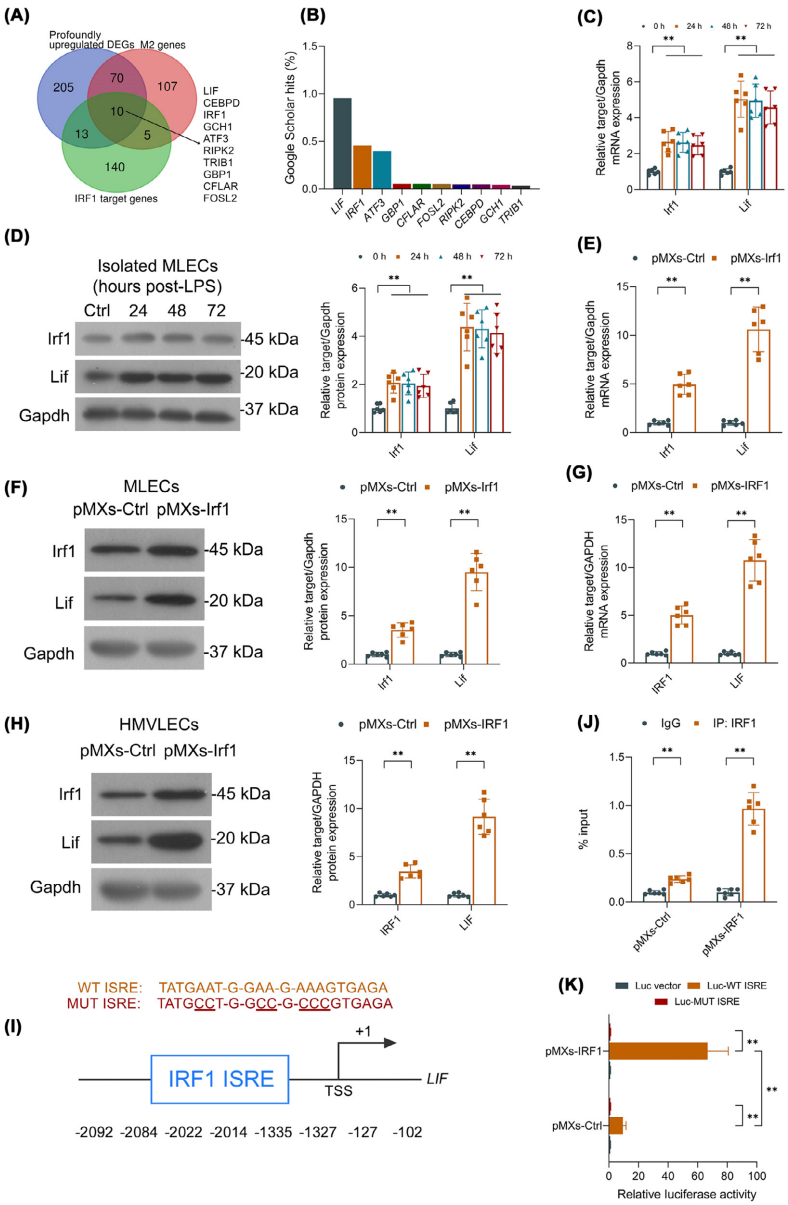

Figure 2. LPS induces Irf1-mediated Lif transactivation in lung endothelial cells

(**A**) Venn analysis identifying profoundly up-regulated Irf1 target genes in murine lung endothelial cells (MLECs). (**B**) Web-based term association analysis to identify which Irf1 target gene(s) have the strongest association with endothelial regeneration-associated search terms. (**C**) qPCR analysis of Irf1 and Lif gene expression in MLECs isolated from mice pre- and post-LPS. (**D**) Representative immunoblots and densitometric quantification of Irf1 and Lif protein levels in MLECs pre- and post-LPS challenge. (**E**) qPCR analysis of IRF1 and LIF gene expression in human lung microvascular endothelial cells (HLMVECs) isolated from mice pre- and post-LPS. (**F**) Representative immunoblots and densitometric quantification of IRF1 and LIF protein levels in HLMVECs pre- and post-LPS challenge. (**G**) qPCR analysis of IRF1 and LIF gene expression in human lung microvascular endothelial cells (HLMVECs) transfected with control or IRF1 vector. (**H**) Representative immunoblots and densitometric quantification of IRF1 and LIF protein levels in HLMVECs with control vector or IRF1 overexpression. (**I**) Schematic of the human *LIF* promoter region depicting the highly-conserved IRF1 ISRE binding site at −102 ∼ −127 bp. The WT and MUT ISRE sequences used in panel (**K**) are provided. (**J**) HLMVECs transduced with either control or IRF1 plasmids, subjected to vehicle or LPS conditions for 8 h, followed by ChIP-qPCR assays for detection of IRF1 binding to the −102 bp binding site within the *LIF* promoter region. (**K**) HLMVECs co-transfected with control or IRF1 plasmid along with one of three luciferase (Luc) reporter gene constructs. Schematic representations of Luc constructs are indicated. All experiments: $n = 6$ mice or six independent biological replicates per group. Data represented as means ± SDs. $^{**}P<0.01$ [one-way ANOVA (C) and two-way ANOVA (E–H) with Bonferroni post-hoc tests].

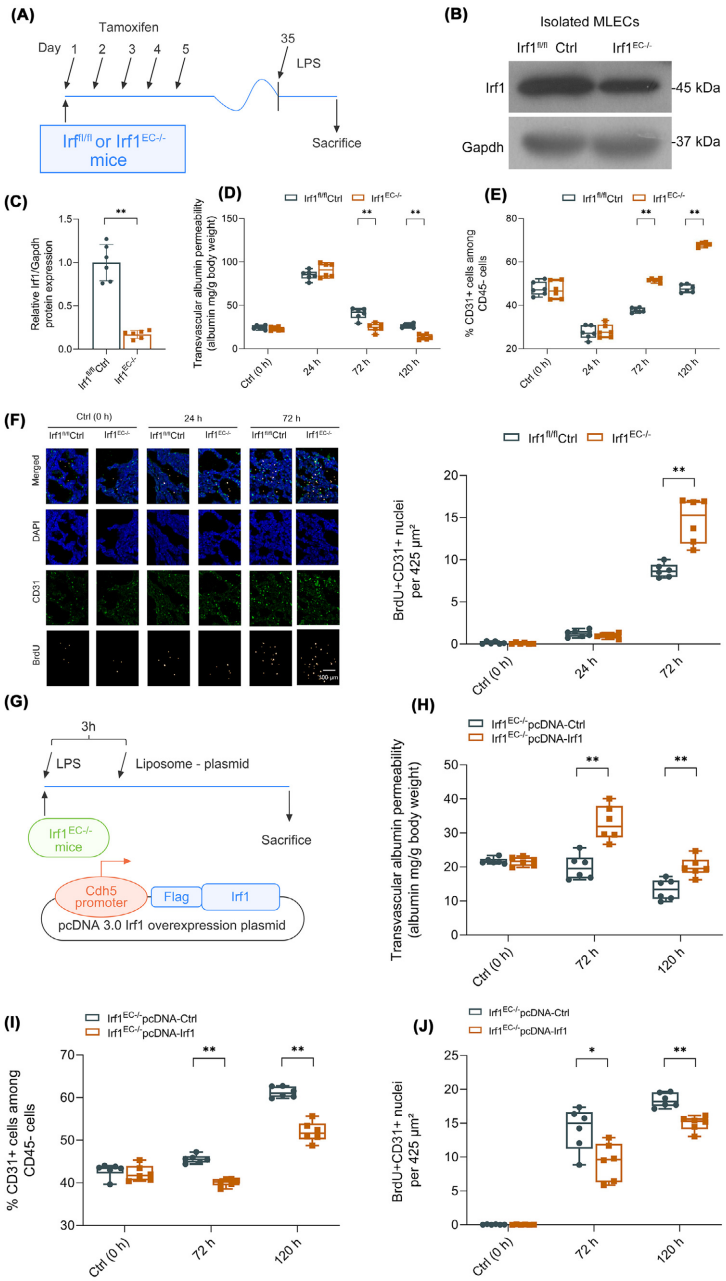

Figure 3. Endothelial *Irf1* knockout in mice inhibits lung endothelial cell regeneration

(**A**) Schematic illustration depicting *Irf1*$^{fl/fl}$ × *Cdh5*-CreERT2 mice crosses to construct endothelial cell-specific Irf1 knockout mice (*Irf1*$^{EC-/-}$). Tamoxifen was administered for five consecutive days, left to rest for 4 weeks prior to a sub-lethal (8 mg/kg) LPS challenge. (**B**) Irf1 protein levels in endothelial cells isolated from flushed lungs from control and *Irf1*$^{EC-/-}$ mice. (**C**) Quantification of protein levels. (**D**) Time course illustrating lung vessel permeability post-LPS in control and *Irf1*$^{EC-/-}$ mice. (**E**) Flow cytometric analysis of CD31+CD45− endothelial cells in mice post-LPS injury. (**F**) Representative images of BrdU-APC, CD31-AF488, and DAPI co-staining in lung cryosections obtained from control *Irf1*$^{fl/fl}$ mice and *Irf1*$^{EC-/-}$ mice 3 days post-LPS. BrdU+ MLEC quantification in lung cryosections obtained from mice post-LPS ($n = 10$ cryosections per mouse). (**G**) Re-introduction of *Irf1* through liposome vector plasmids (50 µg) in *Irf1*$^{EC-/-}$ mice post-LPS. (**H**) Lung vessel permeability at day 3 following LPS challenge in *Irf1*$^{EC-/-}$ mice with re-introduced *Irf1*. (**I**) Flow cytometric analysis of CD31+CD45− endothelial cells at day 3 following LPS challenge in *Irf1*$^{EC-/-}$ mice with re-introduced *Irf1*. (**J**) BrdU+ MLEC quantification in lung cryosections obtained at day 3 following LPS challenge in *Irf1*$^{EC-/-}$ mice with re-introduced *Irf1* ($n = 10$ cryosections per mouse). All experiments: $n = 6$ mice or six independent biological replicates per group. Data represented as means ± SDs. $^{*}P<0.05$, $^{**}P<0.01$ [two-tailed Student's *t*-tests (**C, J**) and two-way ANOVA (**D, E–H**) with Bonferroni post-hoc tests, and Log-rank Mantel-Cox tests].

Clinical Science (2023) **137** 367–383
https://doi.org/10.1042/CS20220876

terms 'endothelial" AND ('regeneration' OR 'proliferation' OR 'viability' OR 'maintenance' OR 'apoptosis') AND *gene symbol*, where the *gene symbol* was the target gene symbol of interest. The results were reported as percentage of the total hits for the search terms 'endothelial' AND ('regeneration' OR 'proliferation' OR 'viability' OR 'maintenance OR 'apoptosis').

Mice

All animal-related experiments were performed at Chongqing Medical University (Chongqing, China). Wild-type (WT) C57BL/b mice (strain no. 027) were obtained from Charles River. *Cdh5*-CreERT2 mice (MGI ID: 3848982) were obtained from Taconic Biosciences (model no. 13073) [17]. *Irf1*-floxed ($Irf1^{fl/fl}$) mice (cat. no. NM-CKO-2102684, Shanghai Model Organisms) were crossed with *Cdh5*-CreERT2 mice to create tamoxifen-inducible $Irf1^{EC-/-}$ mice. All animal experiments were conducted with 8- to 12-week-old mice and using age- and sex-matched $Irf1^{fl/fl}$ mice as controls. All mice were kept in a pathogen-free environment and randomly selected for treatment arms by a random number generator with equivalent numbers assigned to each cohort. The animal operators were not blinded to cohort assignments, but investigators responsible for the collection and analysis of data were blinded to cohort assignments.

Generation of the ALI murine model

We employed an endotoxemic murine model of ALI induced by systemic intraperitoneal LPS as previously described [3]. Briefly, mice were fed tamoxifen 20 mg/ml in corn oil) for five consecutive days to induce endothelial cell-specific deletion of *Irf1* before being left untreated for 4 weeks. Thereafter, mice were challenged with phosphate-buffered saline (PBS) vehicle control or a sublethal dose of LPS (8 mg/kg i.p., Ultrapure LPS from *E. coli* 0111:B4; cat. no. tlrl-3pelps, Invivogen) and then killed at various endpoints before tissue harvesting. Mice were anesthetized with pentobarbital sodium (50 mg/kg) and were decapitated.

Assessment of lung inflammation in ALI model mice

Lung inflammation in ALI model mice was assessed 24 h post-LPS administration as previously described [18]. Briefly, bronchoalveolar lavage fluid (BALF) was obtained using 3 × 1 ml PBS lavage (3 ml total volume). At least 2.7 ml (90% of the total volume) was recovered for all subjects. BALF samples were centrifuged (450 ***g***, 10 min), and then neutrophil counts were measured in the BALF cell fraction. The BALF supernatant was used to assess LDH (cat no. LS-F5048), IL-1β (cat no. LS-F5626), and TNF-α levels (cat no. LS-F12798) by ELISA (LSBio).

Whole lungs were excised from the thoracic cavity, weighed in their wet state, dried to a constant dry weight (50°C, 72 h), and then weighed in their dry state. The lung wet-to-dry (W/D) ratio was calculated by dividing the wet lung weight by the dry lung weight. Lungs were frozen and homogenized in ice-cold potassium phosphate buffer with protease inhibitor followed by two cycles of sonication. The lung homogenates were employed to assess MPO activity, a marker of neutrophil sequestration, as previously described [19]. Whole-cell extracts were prepared from lung homogenates using RIPA buffer and subjected to immunoblotting as described below.

Mouse lung cell isolation

Lungs harvested from mice were minced and digested with Type I Collagenase 1 (2 mg/ml) for 1 h at 37°C. Samples were titrated with an 18-gauge needle and strained through a 40 μm cell strainer. Next, samples were centrifuged for 5 min at 300 ***g*** before being washed and treated with red blood cell lysis buffer for 5 min on ice.

Isolation of murine endothelial cell and non-endothelial cell fractions

Following lung cell isolation, cells were incubated with anti-CD31 (5 μg; cat. no. 553370, BD Biosciences) for 20 min at 4°C with gentle rotation. Next, cells were incubated with Dynabeads (25 μl; cat. no. 11035, Invitrogen) for 25 min at 4°C with gentle rotation. Finally, CD31-positive murine lung endothelial cell (MLEC) fraction and the CD31-negative non-endothelial cell fraction were separated using magnetic columns. The non-endothelial cell fraction was then incubated with anti-CD45 microbeads (cat. no. 130-052-301, Miltenyi Biotec) for 20 min at 4°C with gentle rotation to further deplete CD45+ cells. Cell population purity in the CD31+ and CD31−CD45− fractions was assessed by flow cytometry.

Flow cytometric analysis

Following lung cell isolation described above, cells were stained with anti-murine CD16/CD32 (1:50, cat. no. 553142, BD Biosciences) for 10 min to block endogenous Fc receptors. Next, cells were stained with anti-CD31-APC (1:1000,

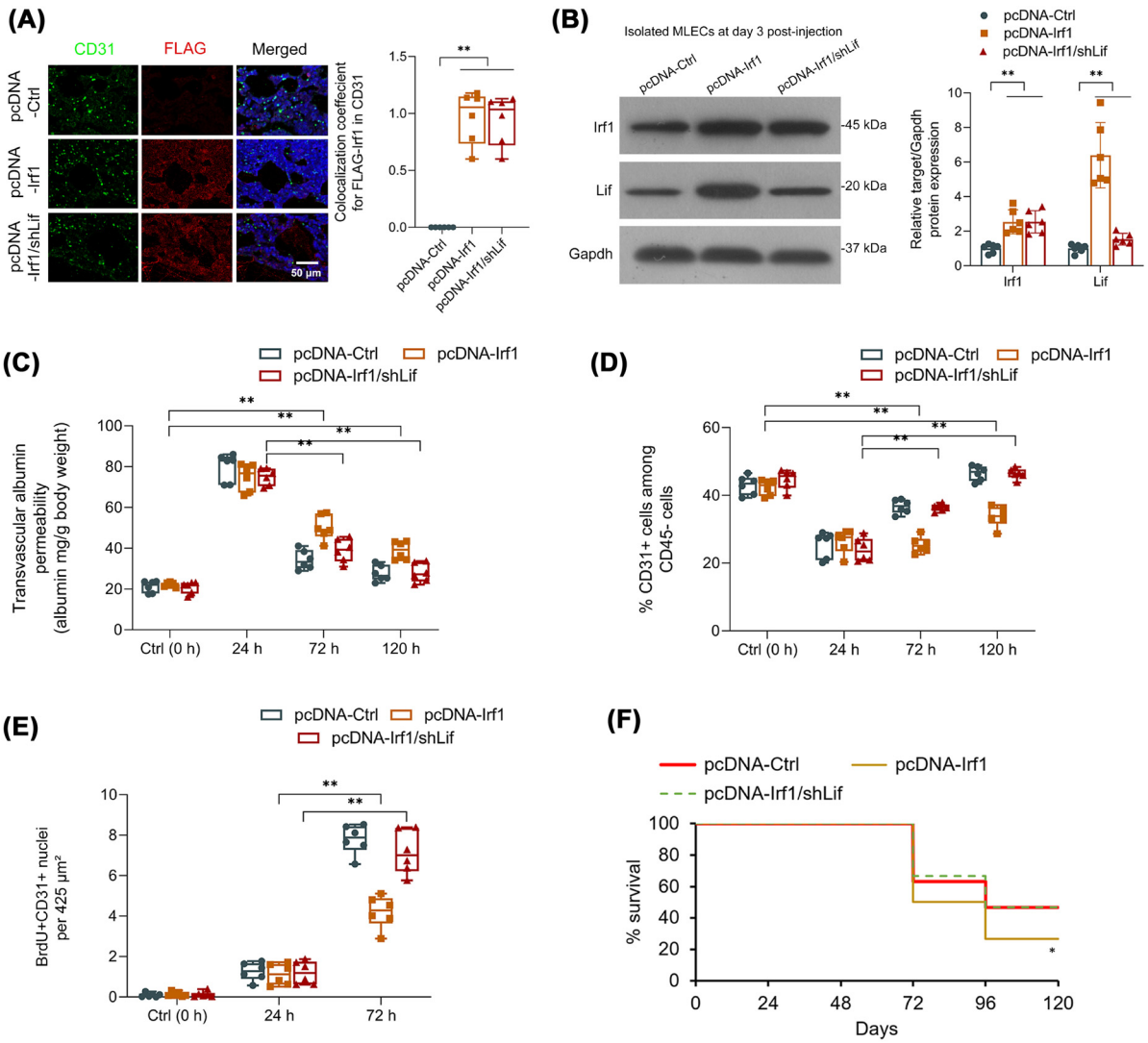

Figure 4. Irf1 overexpression inhibits lung endothelial regeneration in a Lif-dependent manner

(**A**) Confocal microscopy illustrating FLAG staining along with CD31+ and DAPI staining in lung cryosections obtained from mice receiving either a scrambled control (Ctrl), FLAG-*Irf1*, or FLAG-*Irf1*/shLif construct. Scale bar = 50 and 20 µm (enlarged panel). Co-localization coefficient for FLAG-Irf1 staining in CD31+ MLECs. (**B**) FLAG-Irf1 and Lif protein levels in MLECs derived from mice receiving either a Ctrl, FLAG-*Irf1*, or FLAG-*Irf1*/shLif construct. (**C**) Lung vessel permeability pre- and post-LPS in mice receiving either a Ctrl, FLAG-*Irf1*, or FLAG-*Irf1*/shLif construct. (**D**) Flow cytometric analysis of CD31+CD45− endothelial cells pre- and post-LPS in mice receiving either a Ctrl, FLAG-*Irf1*, or FLAG-*Irf1*/shLif construct. (**E**) BrdU+ MLEC quantification in lung cryosections obtained from mice receiving either a Ctrl, FLAG-*Irf1*, or FLAG-*Irf1*/shLif construct ($n = 6$ cryosections per mouse). (**F**) Survival curves following LPS challenge in mice receiving either a Ctrl, FLAG-*Irf1*, or FLAG-*Irf1*/shLif construct ($n = 30$ mice per group). All experiments except (F): $n = 6$ mice or six independent biological replicates per group. Data represented as means ± SDs. $^{*}P<0.05$, $^{**}P<0.01$ [(A–E) two-way ANOVA with Bonferroni post-hoc test; (F) Log-rank test].

cat. no. 17-0311-82, eBiosciences) and anti-CD45-EF450 (1:2000, cat. no. 48-0451-82, eBiosciences) at 4°C for 45 min. Finally, cells were resuspended in 500 µl of FACS buffer, and data were acquired on a MoFlo Astrios instrument (Beckman Coulter). The flow cytometry data were analyzed using Summit (Beckman Coulter).

Cell culture

Isolated MLECs and HLMVECs (cat. no. CC-2527, Lonza) were cultured in complete Clonetics EGM-2MV BulletKit Media (Lonza) supplemented with 15% FBS and kept at 37°C and 5% CO_2. To induce $STAT1^{Ser727}$ phosphorylation,

Clinical Science (2023) **137** 367–383
https://doi.org/10.1042/CS20220876

endothelial cells were incubated with PBS vehicle control or 10 μg/ml Ultrapure LPS (Invivogen) for 30 min as previously described [14]. 293T cells were obtained from ATCC and cultured in DMEM media (Gibco) supplemented with 10% FBS and kept at 37°C and 5% CO_2.

RNA extraction and qPCR

TRIzol (ThermoFisher) was used to extract total RNA from cells as per the manufacturer's protocol. NanoDrop 1000 was used to quantify RNA content and the High-Capacity RNA Transcription Kit (ThermoFisher) was used to generate complementary DNA (cDNA). FastStart SYBR Green MasterMix (ThermoFisher) was used for qPCR detection on the ViiA 7 RT PCR System (ThermoFisher). All primers were purchased from Origene; the primer sequences are available in Supplementary Table S1.

Immunoblotting

Following cell isolation, cells were lysed using RIPA buffer (Sigma) supplemented with protease and phosphatase inhibitors (Sigma). DC Protein Assay Kit II was used to quantify protein content in a microplate spectrophotometer. Protein samples were subjected to SDS-PAGE (BioRad) and immunoblotting was conducted using anti-LIF (diluted 1:200; cat. no. ab113262, Abcam), anti-IRF1 (diluted 1:1000; cat. no. PA5-50512 Invitrogen), anti-phospho-NF-κB^{Ser536} (diluted 1:1000; cat. no. 3033, CST), anti-NF-κB (diluted 1:1000; cat. no. 4764, CST), anti-phospho-STAT1^{Ser727} (diluted 1:1000; cat. no. 9177, CST), anti-STAT1 (diluted 1:1000; cat. no. 9172, CST), anti-FLAG M2 (diluted 1:1000; cat. no. F1804, Sigma), and anti-GAPDH loading control (diluted 1:1000; cat. no. ab181602, Abcam). Blots were incubated with HRP-conjugated secondary antibody (diluted 1:2000; CST) for 1 h and treated with ECL substrate (SuperSignal West Pico Chemiluminescent Substrate, ThermoFisher). ImageJ was used for densitometric analysis of protein bands.

Cell proliferation assays

To measure cell proliferation, mice were injected intraperitoneally with BrdU (150 mg/kg; Sigma) and left for 14 h before being scarified. Next the lungs were harvested, washed with PBS, and fixed with OCT (70%) before being frozen at −80°C and later sectioned for tissue histology.

Pulmonary transvascular permeability assays

Evans blue-albumin tracing for pulmonary transvascular permeability was conducted as previously described [3]. The right jugular vein of ketamine-xylazine anesthetized mice was injected with 8 μl/g body weight Evans Blue–albumin (40 mg/ml BSA containing 1% Evans blue dye, Sigma) and left to circulate for 45 min. A 2-min PBS perfusion into the right ventricle was used to wash out the intravascular Evans Blue. Lungs were excised, homogenized in PBS (1 ml), and extracted using formamide (2 ml) at 60°C overnight. A Shimadzu 1650 PC UV-vis spectrophotometer (Kyoto, Japan) was used to measure Evans Blue content at OD620 and normalized against body weight.

Immunofluorescence and confocal microscopy

Frozen tissue sections were paraformaldehyde (4%) fixed and permeabilized using Triton X-100 (0.25%). Following a PBS-Tween-20 wash, slides were incubated with hydrochloric acid (3 M) for 10 min in order to open the nucleus. Next, donkey serum (10%) in BSA (2%) was used to block unspecific bindings during a 1 h incubation at room temperature. Afterward, the following primary antibodies were used to stain the slides during an overnight incubation at 4°C: CD31 (diluted 1:50; cat. no. PA5-16301, Invitrogen), BrdU (diluted 1:100; cat. no. B35128, Invitrogen), and anti-FLAG M2 (diluted 1:100; cat. no. F1804, Sigma). The following day, slides were PBS-washed and stained with fluorescent secondary antibodies (Invitrogen) for 45 min. During the final five minutes of secondary antibody incubation, nuclei were counter-stained with 4′,6′-diamidino-2-phenylindole (DAPI). Cells were PBS-washed and mounted using Vecta Shield mounting medium (Vector Laboratories). Slides were imaged on an LSM710 confocal laser-scanning microscope (Zeiss) and analyzed using Zen software (Zeiss).

Gene overexpression and silencing plasmids

For *in vitro* gene overexpression, the pMXs-ms-*Irf1*, pMXs-ms-*IRF1*, pMXs-ms-*Stat1*, and pMXs-ms-*STAT1* plasmids were generated by respectively cloning the mouse *Irf1* cDNA clone (NM_008390, cat. no. MC200482, Origene), human *IRF1* cDNA clone (NM_002198, cat. no. SC118744, Origene), murine *Stat1* cDNA clone (BC004808, cat no. MC200236, Origene), or human *STAT1* cDNA clone (NM_007315, cat. no. SC115595, Origene) into the pMXs-GW backbone (plasmid 18656, Addgene). Site-directed mutagenesis (BBI Life Science, Shanghai, China) was

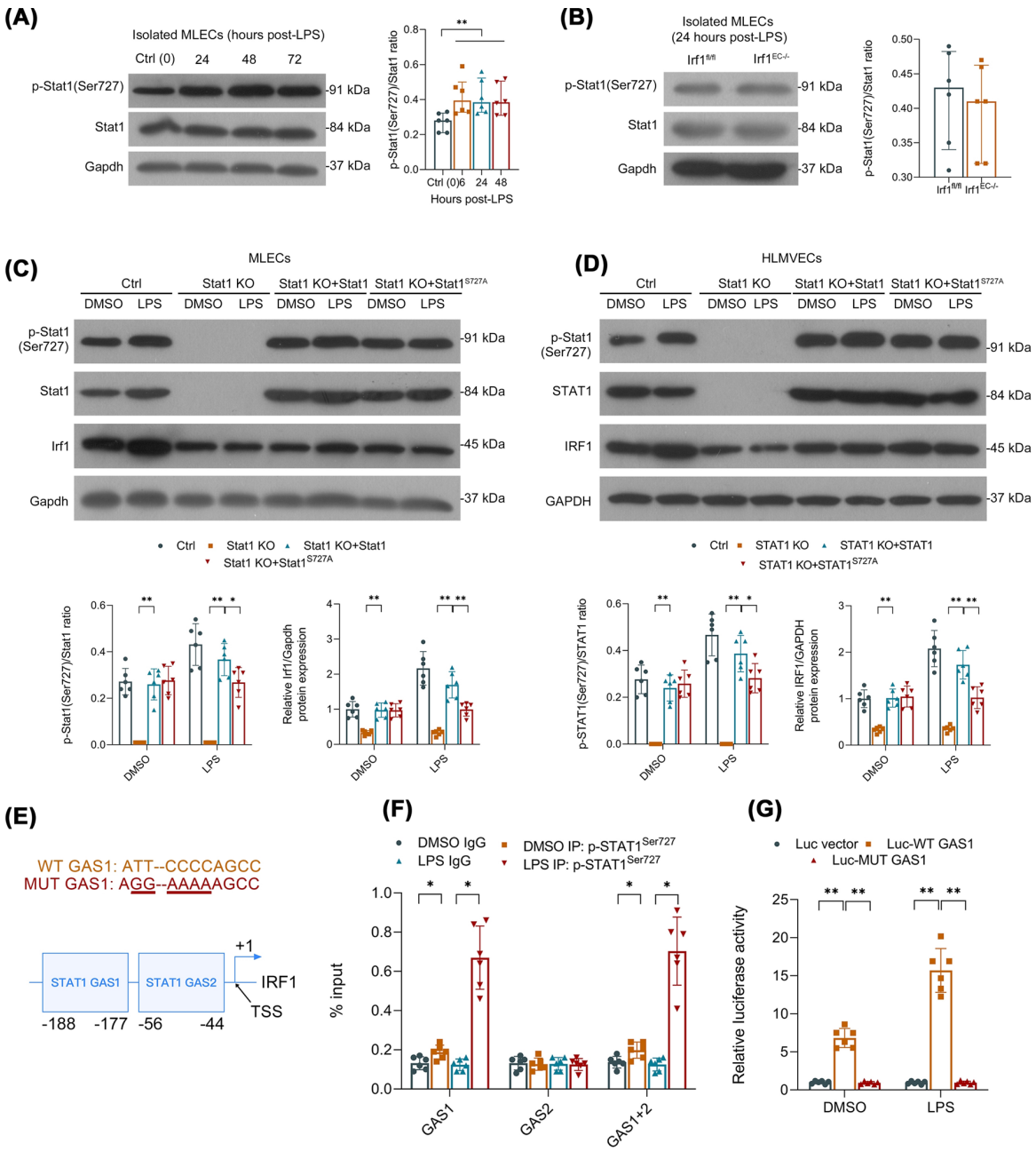

Figure 5. Stat1 signaling transactivates Irf1 in lung endothelial cells

(**A**) Representative immunoblots and densitometric quantification of Stat1^{Ser727} phosphorylation levels in MLECs isolated from *Ifr1*$^{fl/fl}$ control mice pre- and post-LPS. (**B**) Representative immunoblots and densitometric quantification of Stat1^{Ser727} phosphorylation levels in MLECs in *Ifr1*$^{fl/fl}$ control mice and endothelial cell-specific *Irf1* knockout mice at baseline. (**C**) Representative immunoblots and densitometric quantification of Stat1^{Ser727} phosphorylation and Irf1 protein levels in the indicated MLEC cell lines following LPS (10 μg/ml) treatment. (**D**) Representative immunoblots and densitometric quantification of STAT1^{Ser727} phosphorylation and IRF1 protein levels in the indicated HLMVEC cell lines following LPS (10 μg/ml) treatment. (**E**) Schematic of the human *IRF1* promoter region depicting the two highly-conserved STAT1 binding site at −44 ∼ −56 bp and −177 ∼ −188 bp. The WT and MUT GAS1 sequences used in panel (**G**) are provided. (**F**) HLMVECs subjected to vehicle or LPS conditions for 8 hours, followed by ChIP-qPCR assays for detection of STAT1 binding to the two binding sites within the *IRF1* promoter region. (G) HLMVECs co-transfected with control or STAT1 plasmid along with one of three luciferase (Luc) reporter gene constructs. Schematic representations of Luc constructs are indicated. All experiments: $n = 6$ mice or 6 independent biological replicates per group. Data represented as means ± SDs. $^{*}P<0.05$, $^{**}P<0.01$ [(A, C, D) one-way ANOVA with Bonferroni post-hoc tests, and Log-rank Mantel-Cox tests; (B) two-tailed Student's *t*-tests; (E, H, I) two-way ANOVA with Bonferroni post-hoc tests].

Clinical Science (2023) **137** 367–383
https://doi.org/10.1042/CS20220876

performed on the pMXs-ms-*Stat1* and pMXs-ms-*STAT1* plasmids to create the non-phosphorylable mutant plasmids pMXs-ms-*STAT1*^{S727A} and pMXs-ms-*Stat1*^{S727A}, respectively [20]. The empty pMXs-GW vector was used as a negative control.

For *in vivo* endothelial gene overexpression and silencing in mice, the murine *Cdh5* promoter region described by Gory et al. (2.5-kb fragment, −2486/+24 [21]) was cloned from mouse gDNA and inserted into a pcDNA 3.0 vector (Invitrogen) to form the pcDNA-*Cdh5* vector. Next, the murine *Irf1* cDNA clone (NM_008390, cat. no. MC200482, Origene) was inserted into the pcDNA-*Cdh5* vector. The *Irf1* coding region (N-terminus) was bound to a FLAG tag (GAC TAC AAA GAC GAT GAC GAC AAG) to form the pcDNA-*Cdh5*-FLAG-*Irf1* construct. A small hairpin RNA (shRNA) against murine Lif (shLif, sc-37223-SH, SCBT) was annealed into the Bbs I-Xba I site of the mU6pro plasmid as previously described [22]. This mU6pro-shLif construct was then ligated into the pcDNA-*Cdh5*-FLAG-*Irf1* plasmid to create the pcDNA-*Cdh5*-FLAG-*Irf1*/shLif plasmid. The empty pcDNA-*Cdh5* vector was used as a negative control.

To conduct the liposome-*EGFP* gene biodistribution experiment, the coding region of the EGFP protein as amplified using the pWPXL plasmid and inserted in the pcDNA-*Cdh5* vector.

In silico promoter analyses

We analyzed the 1000-bp promoter regions upstream of the transcription start sites (TSS) for the human *LIF* and *IRF1* genes using the ConTra v3 tool [23]. Using the JASPAR CORE 2016 database selection in the ConTra v3 tool, the predicted IRF1-binding sites within the *LIF* promoter region were identified through the IRF1 IFN-stimulated response elements (ISRE) motif MA0050.2 [24], and the predicted STAT1-binding sites within the *IRF1* promoter region were identified through the STAT1 IFN-Gamma Activated Site (GAS) motif MA0137.3 [25].

Chromatin immunoprecipitation coupled with quantitative PCR (ChIP-qPCR)

For ChIP-qPCR of IRF1 binding to the human *LIF* promoter, HLMVECs were transfected with pMXs-ms-*IRF1*, then crosslinked with formaldehyde (1%) before being washed with PBS three times, then resuspending in lysis buffer. To break down the DNA, nuclear lysis buffer was added to the nuclear fraction and samples were sonicated suing a focused-ultrasonicator (covaries). Following centrifugation, sample supernatants were incubated with anti-IRF1 (5 μg) for immunoprecipitation. DNA isolated via immunoprecipitation was subjected to qPCR using primers that bind to specific IRF1 ISRE binding site within the *LIF* promoter region (Supplementary Table S1). For ChIP-qPCR of p-STAT1^{Ser727} binding to the human *IRF1* promoter, HLMVECs were subjected to PBS vehicle control or 10 μg/ml Ultrapure LPS (Invivogen) before the above protocol was followed using anti-p-STAT1^{Ser727} (5 μg) for immunoprecipitation and qPCR primers that bind to identified STAT1 GAS binding sites within the *IRF1* promoter region (Supplementary Table S1).

Dual-luciferase reporter assays

For the *LIF* promoter experiments, the WT human *LIF* promoter clone (1608-bp fragment, -1450/+157; HPRM39845, GeneCopoeia) or its IRSE mutant (MUT IRSE) was subcloned into the pGL3 Firefly Luciferase (pGL3-Luc) vector (cat. no. E1751, Promega). See Figure 2I for WT IRSE and MUT IRSE sequences. For the *IRF1* promoter experiments, the WT human *IRF1* promoter clone (1562-bp fragment, -1379/+182; HPRM44152, GeneCopoeia) or its GAS1 mutant (MUT GAS1) were subcloned into the pGL3-Luc vector. See Figure 5E for WT GAS1 and MUT GAS1 sequences. Mutants were constructed using a site-directed mutagenesis kit (BBI Life Science, Shanghai, China).

Dual-luciferase reporter assays in HLMVECs were performed as previously described [26]. Briefly, HLMVECs (3×10^5 cells/well) were cultured for 24 h in 500 μl serum-free RPMI-1640 and then co-transfected for 5 h with 0.5 μg pGL3-Luc reporter construct and 0.05 μg control pRL-TK plasmid (cat. no. 2241, Promega) using Lipofectamine 3000 (Invitrogen). The transfected HLMVECs were washed with PBS and incubated for 12 h in normal growth medium. Then, HLMVECs were synchronized in serum-free medium for an additional 12 h. For some experiments, cells were incubated with 10 μg/ml Ultrapure LPS (Invivogen) for this 12-h period. Cells were then lysed to allow for relative luciferase activity (i.e., pGL3-Luc reporter luciferase activity / pRL-TK reporter luciferase activity) to be calculated via the Dual-Luciferase Reporter Assay Kit (Promega) on the FloMax luminometer (Promega).

CRISPR/Cas9-based STAT1 knockout

The following sgRNA sequences targeting murine *Stat1* and human *STAT1* for CRISPR/Cas-9 mediated deletion were derived from the GPP sgRNA Designer tool (https://portals.broadinstitute.org/gpp/public/analysis-tools/sgrna-design) and a previously published work [27], respectively: murine *Stat1*, 5′-TGCAAAACCTCTCAGAACAG-3′ and 5′-TGTGATGTTAGATAAACAGA-3′; human *STAT1*, 5′-TCATGACCTCCTGTCACAGC-3′ and 5′-GAGGTCATGAAAACGGATGG-3′. Lentiviral STAT1 sgRNA and adenoviral Cas9 transduction of MLECs and HLMVECs were conducted as previously reported [3]. Briefly, PCR products were cloned into the pLX-single sgRNA lentiviral plasmid (plasmid 50662, Addgene). Preparation of lentiviral particles was done through co-transfections of psPAX2 (plasmid 12260, Addgene) and pMD2-G (plasmid 12259, Addgene) into 85–90% confluent 293T cells with Lipofectamine 3000 reagent as per the manufacturer's protocol. Supernatants containing the lentiviral particles were collected at 72 h post-transfection, concentrated, and then infected into the cells in the presence of polybrene (8 μg/ml; Sigma) at a Multiplicity of Infection (MOI) of 10. At 8 h post-infection, EGFP-tagged Cas9 adenovirus (Ad-GFP-Cas9, cat. no. 1901, Vector Biolabs) was then infected into the cells in the presence of polybrene (8 μg/ml) at a MOI of 10. After 2–3 days of incubation, cells were trypsinized and split in a 1:3 ratio in order to receive another round of lentivirus and adenovirus infections. After an additional 2–3 days of incubation, cells were used for downstream experiments.

Lung endothelial cell liposome gene delivery

Liposomal-based gene delivery to lung endothelium was performed as previously described [3]. Briefly, dimethyldioctadecylammonium bromide and cholesterol were dissolved in chloroform to a ratio of 1:1. Chloroform was evaporated via centrifugation at 37°C for 20 min. Then, dried lipid was resuspended in dextrose (5%) in water, sonicated for 20 min, and filtered using a 0.45 or 0.22 μm strainer. These steps were used to reduce the polydispersity index (PDI), a measurement of liposome size distribution ranging from 0 to 1 [28–30]. Size (Supplementary Figure S1A,B), PDI (Supplementary Figure S1C,D), and surface charge (Supplementary Figure S1E) were measured using dynamic light scattering (Zetasizer Nano).

For our *in vivo* experiments, we employed only 0.22-μm strained liposomes (DDAB/cholesterol) with a high charge ratio (+4.5, +fatty acid/-DNA). The DNA complex consisted of FLAG-tagged *Irf1* coding region following the endothelial cell-specific mouse *Cdh5* promoter to ensure endothelial cell transgene expression [17]. Anesthetized mice were then retro-orbitally injected with the liposome-DNA complex (50 μg DNA:100 μg liposome). *In vivo* liposome-*EGFP* gene biodistribution was measured using dynamic light scattering (Zetasizer Nano). In line with previous reports [31,32], our liposomal formulations resulted in disproportionate overexpression of the *EGFP* transgene in lung endothelial cells (Supplementary Figure S1F).

Statistics

Data represented as means ± standard deviations (SDs) unless otherwise specified. To determine statistical significance, Student's *t*-tests, one- and two-way analysis of variance (ANOVA) with Bonferroni post-hoc tests were used where indicated. A *P*-value of <0.05 was considered significant for all analyses.

Results

R-based bioinformatics analysis identifies Irf1 as a key up-regulated gene in LPS-exposed murine lung endothelial cells

To assess the molecular mechanisms of lung endothelial cell regeneration under inflammatory conditions, R-based CemiTool package were used to analyze microarray-derived transcription profiles in human lung microvascular endothelial cells (HLMVECs) subjected to non-treatment or LPS exposure. The CemiTool GSEA detected three distinct co-expressed gene modules, two of which (M1 and M2) were significantly enriched in the LPS-exposed HLMVECs compared with control HLMVECs based on their normalized enrichment scores (NES) (Figure 1A and Supplementary Table S2). The M1 module contained 594 non-unique gene probes with RPS27A and UBC as prominent hub genes, while M2 contained 246 non-unique gene probes with NFKB1 and CEBPB as prominent hub genes (Figure 1B). From our Reactome over-representation analysis, M1 was most enriched for eukaryotic translation-associated pathways, while M2 was most enriched for interleukin signaling-associated pathways (Figure 1C).

Filtering and quantile normalization of genes (Supplementary Figure S2A–C) followed by moderated *t*-testing using the R-based limma package identified 655 DEGs. To visualize the overall profile of DEGs, we used a volcano plot with staining for M1 and M2 module membership and observed that 113/655 DEGs (17%) were M2 members but only 2/655 DEGs (0.3%) were M1 members (Figure 1D). Moreover, we identified 298 profoundly up-regulated DEGs

Clinical Science (2023) **137** 367–383
https://doi.org/10.1042/CS20220876

($\log_2$FC>1.0) in LPS-exposed HLMVECs relative to control HLMVECs, of which 80/298 (27%) were M2 members and only 1/298 (0.3%) were M1 members. As the M2 module possessed a greater proportion of DEGs relative to the M1 module, we selected the M2 module for further analysis. We used heatmap analysis to identify the 50 most upregulated M2 DEGs in LPS-exposed HLMVECs (Figure 1E). Consistent with our initial hypothesis, we discovered IRF1 to be a profoundly up-regulated M2 DEG. Given IRF1's role as a key transcription factor that coordinates endothelial gene expression under pro-inflammatory stimuli [12], we chose to pursue further investigation on IRF1.

Lung endothelial IRF1 and LIF up-regulated by LPS *in vitro* and *in vivo*

We focused on the role of IRF1 transcriptional targets in regulating endothelial regeneration. We performed an *in silico* Venn analysis to identify profoundly up-regulated M2 DEGs in LPS-exposed HLMVECs that are also ChIP-verified IRF1 target genes [13]; this Venn analysis identified ten IRF1 target genes (Figure 2A). We performed a Web-based term association analysis to identify which of these ten gene(s) have the strongest association with the search terms 'endothelial' AND ('regeneration' OR 'proliferation' OR 'viability' OR 'maintenance' OR 'apoptosis'), which identified the IL-6 family cytokine Leukemia Inhibitory Factor (LIF) (Figure 2B). LIF has been shown to inhibit endothelial proliferation *in vitro* by inhibiting progression into S-phase [33]. Follow-up qPCR in MLECs isolated from WT mice lungs at various time point post-LPS also revealed an up-regulation in Irf1 and Lif compared with control PBS-injected MLECs (Figure 2C). At the protein level, Irf1 and Lif levels were found to be higher in post-LPS MLECs when compared with control MLECs (Figure 2D). This evidence demonstrates that LPS exposure promotes IRF1–LIF signaling in endothelial cells.

To investigate the role of IRF1 on LIF transactivation in endothelial cells independent of LPS, we employed MLEC and HLMVEC cell lines with or without overexpression of *IRF1*. qPCR and immunoblotting revealed Lif mRNA and protein up-regulation in *Irf1*-overexpressing MLECs relative to control MLECs (Figure 2E,F). We found a similar pattern of findings in HLMVECs (Figure 2G,H). Using *in silico LIF* promoter analysis based on the JASPAR CORE 2016 IRF1 ISRE motif (Supplementary Figure S3A–C), one highly conserved, IRF1 ISRE-binding site was identified $-102 \sim -127$ bp upstream of the *LIF* TSS (Figure 2I). ChIP-qPCR assays conducted in HLMVECs demonstrated enhanced IRF1 binding to the −102 bp site with *IRF1* overexpression (Figure 2J). Through the use of dual-luciferase promoter reporter assays in *IRF1*-overexpressing HLMVECs, we found enhanced *LIF* luciferase activity with the WT IRF1 ISRE-binding site with *IRF1* overexpression (Figure 2K). However, there was no impact on *LIF* luciferase activity with a mutated IRF1 ISRE-binding site. Consequently, IRF1 binding at this IRF1 ISRE-binding site within the *LIF* promoter seems to be vital for IRF1-mediated *LIF* transactivation. These data demonstrate that IRF1 promotes LIF transactivation in endothelial cells.

Endothelial cell-specific *Irf1* knockout prevents lung endothelial regeneration

We employed a LPS-induced endotoxemic murine model of ALI. We confirmed that i.p. LPS administration produced several features characteristic of ARDS at one day post-LPS challenge, including enhanced lung injury (assessed by BALF LDH levels; Supplementary Figure S4A), pulmonary edema (assessed by the lung W/D ratio; Supplementary Figure S4B), lung neutrophil infiltration (assessed by lung homogenate MPO activity; Supplementary Figure S4C), BALF neutrophil counts (Supplementary Figure S4D), BALF expression of the inflammatory mediators TNF-α and IL-1β (Supplementary Figure S4E,F), and activation of the key inflammatory transcription factor NF-κB in BALF (Supplementary Figure S4G).

In order to examine the role of Irf1 in this endotoxemic murine model of ALI, we generated endothelial cell-specific *Irf1* knockout ($Irf1^{EC-/-}$) mice using the *Cdh5*-CreERT2 mouse strain [17]. Following cross-breeding, mice were given daily doses of tamoxifen (80 mg/kg) for five consecutive days to induce *Irf1* knockout. The endotoxemic murine model of ALI was conducted after a 4-week period, when endothelial *Irf1* was successfully deleted (Figure 3A). Protein levels were examined to confirm Irf1 knockdown in $Irf1^{EC-/-}$ MLECs (Figure 3B,C). All control $Irf1^{fl/fl}$ mice and $Irf1^{EC-/-}$ mice survived the sublethal dose of LPS (8 mg/kg). There was no significant differences in body weight between the cohorts pre- and post-LPS (Supplementary Table S3A). At one day post-LPS challenge, lung vascular permeability was elevated in both $Irf1^{EC-/-}$ mice and control $Irf1^{fl/fl}$ mice (Figure 3D); therefore, *Irf1* knockout had no impact on the initial severity of LPS-induced endothelial injury. However, at days 3 and 5, $Irf1^{EC-/-}$ mice had a lower degree of endothelial permeability relative to control $Irf1^{fl/fl}$ mice, demonstrating an improved regenerative response. Flow cytometric analysis of isolated MLECs revealed that both $Irf1^{EC-/-}$ mice and control $Irf1^{fl/fl}$ mice had a dramatic loss of MLECs immediately after LPS challenge (Figure 3E). The number of MLECs in control $Irf1^{fl/fl}$ mice

was restored to normal by day 5; however, MLEC counts were restored faster in *Irf1*$^{EC-/-}$ mice. Next, MLEC proliferation was examined via BrdU injections 14 hours prior to sacrifice. Tissue immunohistochemistry and fluorescence demonstrated a significant increase in the number of BrdU-positive MLECs (i.e., BrdU+CD31+ cells) in *Irf1*$^{EC-/-}$ mice 3 days post-LPS when compared with control *Irf1*$^{fl/fl}$ mice (Figure 3F).

Next, we examined whether re-introduction of *Irf1* into *Irf1*$^{EC-/-}$ mice could reduce the regeneration of injured lung endothelium. To do so, an endothelial-specific pcDNA-*Cdh5*-FLAG-*Irf1* plasmid was introduced through liposomal biodelivery 3 h post-LPS challenge (Figure 3G) as previously described [3]. Efficacy and specificity of liposomal biodelivery was determined by measuring FLAG-*Irf1* expression in MLECs in comparison with control MLECs and non-MLECs (Supplementary Figure S5). There was no significant differences in body weight between the cohorts pre- and post-LPS (Supplementary Table S3B). Liposomal re-introduction of *Irf1* led to reduced regeneration of the lung endothelial barrier in comparison with control vector (Figure 3H). Flow cytometric analysis of isolated MLECs revealed that liposomal re-introduction of *Irf1* reduced the number of MLECs in comparison with control vector (Figure 3I). MLEC proliferation examined via BrdU injections 14 h prior to sacrifice demonstrated a significant decrease in the number of BrdU-positive MLECs in *Irf1* vector mice when compared with control vector mice (Figure 3J).

Irf1 promotes murine lung endothelial degradation and mortality in a Lif-dependent manner

Next, we examined whether introduction of shRNA-mediated Lif knockdown in WT mice could rescue the destructive effects of artificial *Irf1* overexpression on the lung endothelium. The empty pcDNA-*Cdh5* control vector, pcDNA-*Cdh5*-FLAG-*Irf1*, or pcDNA-*Cdh5*-FLAG-*Irf1*/shLif plasmid constructs encapsulated in cationic liposomes were injected into WT mice 3 h post-LPS challenge to induce artificial *Irf1* overexpression with or without shRNA-mediated Lif knockdown within the lung endothelium. There was no significant differences in body weight between the cohorts pre- and post-LPS (Supplementary Table S3C). On day 3 post-injection, FLAG-CD31 co-localization could be seen in the *Irf1* and *Irf1*/shLif cohorts (Figure 4A). Immunoblotting in isolated MLECs revealed Irf1 and Lif up-regulation in *Irf1* mice, but Irf1 up-regulation and Lif knockdown in *Irf1*/shLif mice, at 3 days post-injection (Figure 4B). The shLif construct showed a 75% Lif knockdown efficacy. We also observed degradation of the lung endothelial barrier and MLEC loss in *Irf1* mice relative to control mice (Figure 4C,D). Levels of BrdU+ endothelial cells were decreased in *Irf1* mice relative to control mice (Figure 4E), demonstrating proliferative retardation in the lung endothelial barrier. Consistently, we also observed reduced survival in *Irf1* mice (Figure 4F). These effects were abrogated in *Irf1*/shLif mice, indicating that Lif mediates Irf1's destructive effects on the lung endothelium.

Stat1 signaling transactivates Irf1 in lung endothelial cells

Having discovered the destructive effects of the Irf1/Lif axis on lung endothelial regeneration, we next focused on the upstream regulation of Irf1 expression in lung endothelial cells. LPS has been shown to enhance STAT1^{Ser727} phosphorylation in aortic endothelial cells [14]. Therefore, we examined Stat1^{Ser727} phosphorylation in isolated MLECs from *Irf1*$^{fl/fl}$ control mice following LPS-induced injury and found that Stat1^{Ser727} phosphorylation levels were indeed up-regulated (Figure 5A). Moreover, immunoblotting in isolated MLECs from *Irf1*$^{EC-/-}$ mice and *Irf1*$^{fl/fl}$ control mice revealed that endothelial Irf1 knockout had no significant impact on Stat1^{Ser727} phosphorylation levels (Figure 5B), suggesting that p-Stat1^{Ser727} functions upstream of Irf1 in the lung endothelium.

To further investigate the role of p-Stat1^{Ser727} in lung endothelial cells *in vitro*, we constructed guide RNAs to enable CRISPR/Cas9-mediated Stat1 knockout [42] in MLECs and HLMVECs. Stat1-knockout MLECs displayed a 97% Stat1 knockdown efficacy (Figure 5C), while Stat1-knockout HLMVECs displayed a 96% Stat1 knockdown efficacy (Figure 5D). We also transfected these Stat1-knockout cells with either WT Stat1 or non-phosphoryable mutant Stat1^{S727A} overexpression plasmids for Stat1 rescue. In control MLECs, LPS exposure resulted in a significant increase in Stat1^{Ser727} phosphorylation and Irf1 protein levels. However, in Stat1-knockout MLECs, we observed an abrogation in this LPS-induced Irf1 upregulation that was rescued by WT Stat1 overexpression but not mutant Stat1^{S727A} overexpression. We found a similar pattern of findings in HLMVECs. This combined evidence demonstrates that p-Stat1^{Ser727} is necessary for LPS-induced IRF1 up-regulation in lung endothelial cells.

Using *in silico IRF1* promoter analysis based on the JASPAR CORE 2016 STAT1 GAS motif (Supplementary Figure S6A–D), we found two strongly conserved STAT1 GAS binding sites located at −44 ∼ −56 and −177 ∼ −188 upstream of the *IRF1* TSS that we termed STAT1 GAS1 and STAT1 GAS2, respectively (Figure 5E). Previous work

Clinical Science (2023) **137** 367–383
https://doi.org/10.1042/CS20220876

has revealed only one GAS motif that is STAT1-responsive under IFN-independent conditions (namely, TTTCC-CCGAAA) [34]; this sequence corresponds only to the STAT1 GAS1 site, not the STAT1 GAS2 site. Accordingly, ChIP-qPCR assays of the two amplified STAT1 GAS binding sites conducted in HLMVECs demonstrated enhanced STAT1 binding to the STAT1 GAS1 binding site (but not the STAT1 GAS2 binding site) under LPS conditions (Figure 5F). Through the use of dual-luciferase promoter reporter assays in HLMVECs, we found enhanced *IRF1* luciferase activity with the WT STAT1 GAS1 site under LPS conditions. However, LPS exposure had no impact on *IRF1* luciferase activity in HLMVECs with the mutated STAT1 GAS1 binding site (Figure 5G). Consequently, STAT1 binding at the STAT1 GAS1 binding site within the *IRF1* promoter seems to be vital for LPS-induced, STAT1-mediated *IRF1* transactivation.

Discussion

In the present study, we established a role for LPS-induced Stat1^{Ser727} phosphorylation in Irf1 transactivation in lung endothelial cells, resulting in Irf1/Lif-mediated retardation of lung endothelial cell proliferation. These results demonstrate the existence of a p-Stat1^{Ser727}–Irf1–Lif axis that inhibits lung endothelial cell regeneration post-LPS injury. As endothelial cells that survive endotoxin-induced injury become the primary source of endothelial cells that go on to repopulate and restore the vessel [3], targeting this axis may be an effective strategy in maintaining lung endothelial integrity in ARDS patients.

Our understanding of lung endothelial cell regeneration in response to endotoxin-induced inflammation has improved in recent years but still remains unclear. Linage tracing experiments in mice have demonstrated significant endothelial cell loss in lung tissue post-LPS injury [35]. Specifically, the endothelial cell population and permeability of the lung vasculature sharply reduces during the first day following LPS challenge, which then recover progressively within a 7-day period [3]. Here, we first aimed to identify the key molecular player(s) involved in this endothelial restoration. As a recent transcriptomic study of various endothelial cells suggests that regulation of networks and pathways can differ among endothelial cells from distinct vascular beds [36], we specifically focused our R-based bioinformatics analysis on comparing HLMVECs that were untreated or exposed to LPS. This *in silico* analysis identified the transcription factor IRF1 to be a profoundly up-regulated DEG in response to LPS, suggesting that IRF1 may play a role in LPS-induced lung endothelial dysfunction.

In order to investigate the role of IRF1 in endothelial regeneration, we utilized an endothelial-specific *Irf1* knockout (*Irf1*$^{EC-/-}$) mouse model that expresses Cre recombinase fused to a tamoxifen-inducible mutant estrogen ligand-binding domain ERT2 under the control of the endothelial-specific *Cdh5* promoter (*Cdh5*-CreERT2) [17]. At day one following LPS challenge, *Irf1*$^{EC-/-}$ and control *Irf1*$^{fl/fl}$ mouse lungs both displayed increased vascular permeability. However, during the recovery phase, the loss of endothelial *Irf1* resulted in a lower degree of endothelial permeability coupled with increased MLEC counts and proliferation, indicative of an improved regenerative response. Moreover, liposomal re-introduction of *Irf1* into *Irf1*$^{EC-/-}$ mice abrogated this regenerative response. Consistent with our findings, IRF1 has been shown to suppress human arterial endothelial cell proliferation via up-regulating cell growth-inhibiting caspase-1 and down-regulating pro-proliferative cyclin D3 [37]. Moreover, IRF1 has been shown to inhibit VEGF-induced HUVEC proliferation, migration, and invasion as well as Matrigel-based tube formation *in vitro* and vessel sprouting *ex vivo* [38].

In addition to IRF1, there are eight other IRFs expressed in mammals: IRF2-9 [39]. Our R-based bioinformatics analysis in HMVLECs also identified IRF2 and IRF8 as being up-regulated in response to LPS. However, IRF2 and IRF8 were not members of the dysregulated M2 module and, to our knowledge, have no known association with endothelial proliferation or apoptosis. Therefore, these IRFs likely do not play key roles in lung endothelial cell regeneration. All mammalian IRFs possess a conserved DNA-binding domain on their amino terminus with a tryptophan (TRP) cluster recognizing a consensus ISRE element (A/GXGAAAXXGAAACT) [39]. These ISRE elements can be found within the promoters of IFN-stimulated genes [39], suggesting that IRFs can regulate the transactivation of IFN-stimulated genes. Indeed, our *in silico* Venn analysis and follow-up *in vitro* experiments identified the IRF1 target gene LIF, a IFN-inducible cytokine which inhibits endothelial proliferation *in vitro* by inhibiting progression into S-phase [33]. Furthermore, our *in silico LIF* promoter analysis and follow-up *in vitro* experiments confirmed the existence of one highly conserved, putative IRF1 ISRE-binding site necessary for LPS-induced, IRF1-mediated *LIF* transactivation. In order to investigate the role of LIF in endothelial regeneration, we utilized WT mice injected with cationic liposomes containing FLAG-*Irf1* or FLAG-*Irf1*/shLif plasmid constructs post-LPS challenge to induce artificial *Irf1* overexpression with or without Lif knockdown within the lung endothelium. This murine model demonstrated the central role of Lif in mediating Irf1-driven endothelial cell proliferative retardation post-LPS injury.

The observation of Irf1/Lif-driven endothelial cell proliferative retardation in our LPS-induced endoxemic ALI murine model prompted us to examine the upstream regulation of IRF1 expression in lung endothelial cells. Through these studies, we identified LPS-induced STAT1^{Ser727} phosphorylation as a critical upstream regulator of IRF1 transactivation. Furthermore, we identified two strongly conserved STAT1 GAS binding sites within IRF1's promoter region. It is well-established that STAT1 signaling activation via Tyr701 phosphorylation plays a detrimental role in endothelial cells by inhibiting proliferation, increasing inflammatory factor expression, enhancing reactive oxygen species production, and decreasing endogenous NO release [40,41]. As LPS does not impact STAT1^{Tyr701} phosphorylation in endothelial cells [14], we propose that LPS enhances STAT1 DNA-binding activity and IRF1 transactivation through STAT1^{Ser727} phosphorylation, thereby promoting downstream LIF up-regulation and endothelial proliferative retardation.

Despite the involvement of STAT1 signaling in inhibiting endothelial regeneration, direct therapeutic inhibition of STAT1 signaling may be problematic. STAT1 signaling has many pleotropic effects, including the regulation of cell proliferation, apoptosis, stemness, and differentiation [42–44]. Consequently, we believe a better approach would be targeting the pathway downstream through the IRF1–LIF axis. Here, endothelial *Irf1* knockout was shown to augment murine lung endothelial regeneration in addition to improving barrier function and survival rates via Lif. Therefore, direct inhibition of IRF1 or LIF may be a promising strategy for enhancing endothelial cell regeneration and improving clinical outcomes in ARDS patients. Further pre-clinical work is needed to address this possibility.

There are several limitations to the present study. First, the murine model of ALI employed here may not precisely reflect the ARDS phenotype observed in human patients. Second, although our R-based bioinformatics analysis pinpointed IRF1 as a key LPS-induced gene in HLMVECs, other dysregulated genes may play important roles in endothelial regeneration post-LPS injury. Third, although we demonstrated that IRF1 transactivation in lung endothelial cells is directly regulated via STAT1^{Ser727} phosphorylation, other LPS-induced signaling pathways could also contribute to IRF1 upregulation in lung endothelial cells.

To conclude, we show a role for IRF1 in lung endothelial cell regeneration post-endotoxin challenge. IRF1 is transactivated in response to upstream STAT1^{Ser727} phosphorylation, resulting in IRF1/LIF-mediated retardation of lung endothelial cell proliferation. We propose direct inhibition of IRF1 or LIF as a promising therapeutic strategy for improving endothelial barrier regeneration and clinical outcomes in ARDS patients.

Clinical perspectives

- Despite therapeutic advancements, the mortality rate for ARDS patients remains extremely high. Endothelial cell regeneration is crucial in repairing the lung endothelial barrier in ARDS. However, little is known about the molecular mechanism(s) that underpin lung endothelial cell regeneration in ARDS.
- We identified IRF1 as a key upregulated gene in HLMVECs post-LPS exposure. We demonstrated that LPS-induced Stat1Ser727 phosphorylation promotes Irf1 transactivation, resulting in downstream Lif up-regulation that inhibits lung endothelial cell proliferation.
- These results demonstrate the existence of a p-Stat1Ser727-Irf1-Lif axis that inhibits lung endothelial cell regeneration post-LPS injury. Thus, direct inhibition of IRF1 or LIF may be a promising strategy for enhancing endothelial cell regeneration and improving clinical outcomes in ARDS patients.

Data Availability

The data analyzed during this study are available from the corresponding author on reasonable request.

Competing Interests

The authors declare that there are no competing interests associated with the manuscript.

Funding

This work was supported by the National Natural Science Foundation of China [grant number 81670071 (to Daoxin Wang)].

Clinical Science (2023) **137** 367–383
https://doi.org/10.1042/CS20220876

CRediT Author Contribution

Xiaorui Chen: Data curation, Software, Formal analysis, Validation, Investigation, Writing—original draft. **Di Qi:** Conceptualization, Resources, Writing—review & editing. **Shulei Fan:** Data curation, Validation, Investigation, Methodology. **Yirui He:** Data curation, Validation, Investigation, Methodology. **Hekun Jin:** Software, Formal analysis, Investigation. **Daoxin Wang:** Conceptualization, Resources, Data curation, Formal analysis, Supervision, Funding acquisition, Validation, Writing—review & editing.

Ethics Statement

Ethical approval for animal work has been obtained from by the Ethics Committee of the Second Affiliated Hospital of Chongqing Medical University (approval number: 165/2022). All experiments were carried out in line with the NIH guidelines for the Care and Use of Laboratory Animals.

Abbreviations

ALI, acute lung injury; ARDS, acute respiratory distress syndrome; cDNA, complementary DNA; DEG, differentially expressed gene; GSEA, Gene Set Enrichment Analysis; HLMVEC, human lung microvascular endothelial cell; HUVEC, human umbilical vein endothelial cell; IFN, interferon; IRF1, interferon regulatory factor 1; ISRE, IFN-stimulated response element; MLEC, murine lung endothelial cell; MOI, Multiplicity of Infection; NES, normalized enrichment score; PDI, polydispersity index; SD, standard deviation; shRNA, short hairpin RNA; TSS, transcription start sites; WGCNA, weighted correlation network analysis; WT, wild-type.

References

1 Chang, J.C. (2019) Acute respiratory distress syndrome as an organ phenotype of vascular microthrombotic disease: based on hemostatic theory and endothelial molecular pathogenesis. *Clin. Appl. Thrombosis/Hemostasis : Off. J. Int. Acad. Clin. Appl. Thrombosis/Hemostasis* **25**, 1076029619887437, https://doi.org/10.1177/1076029619887437

2 Bellani, G., Laffey, J.G., Pham, T., Fan, E., Brochard, L., Esteban, A. et al. (2016) Epidemiology, patterns of care, and mortality for patients with acute respiratory distress syndrome in intensive care units in 50 countries. *JAMA* **315**, 788–800, https://doi.org/10.1001/jama.2016.0291

3 Liu, M., Zhang, L., Marsboom, G., Jambusaria, A., Xiong, S., Toth, P.T. et al. (2019) Sox17 is required for endothelial regeneration following inflammation-induced vascular injury. *Nat. Commun.* **10**, 2126, https://doi.org/10.1038/s41467-019-10134-y

4 Gu, M., Nguyen, P.K., Lee, A.S., Xu, D., Hu, S., Plews, J.R. et al. (2012) Microfluidic single-cell analysis shows that porcine induced pluripotent stem cell-derived endothelial cells improve myocardial function by paracrine activation. *Circ. Res.* **111**, 882–893, https://doi.org/10.1161/CIRCRESAHA.112.269001

5 Matthay, M.A., Thompson, B.T., Read, E.J., McKenna, Jr, D.H., Liu, K.D. et al. (2010) Therapeutic potential of mesenchymal stem cells for severe acute lung injury. *Chest* **138**, 965–972, https://doi.org/10.1378/chest.10-0518

6 Curley, G.F. and McAuley, D.F. (2015) Stem cells for respiratory failure. *Curr. Opin. Crit. Care* **21**, 42–49, https://doi.org/10.1097/MCC.0000000000000171

7 Curley, G.F., Ansari, B., Hayes, M., Devaney, J., Masterson, C., Ryan, A. et al. (2013) Effects of intratracheal mesenchymal stromal cell therapy during recovery and resolution after ventilator-induced lung injury. *Anesthesiology* **118**, 924–932, https://doi.org/10.1097/ALN.0b013e318287ba08

8 Jia, H., Thelwell, C., Dilger, P., Bird, C., Daniels, S. and Wadhwa, M. (2018) Endothelial cell functions impaired by interferon in vitro: Insights into the molecular mechanism of thrombotic microangiopathy associated with interferon therapy. *Thromb. Res.* **163**, 105–116, https://doi.org/10.1016/j.thromres.2018.01.039

9 Erdmann, J., Vitale, G., van Koetsveld, P.M., Croze, E., Sprij-Mooij, D.M., Hofland, L.J. et al. (2011) Effects of interferons α/β on the proliferation of human micro- and macrovascular endothelial cells. *J. Interferon Cytokine Res.: Off. J. Int. Soc. Interferon Cytokine Res.* **31**, 451–458, https://doi.org/10.1089/jir.2009.0103

10 Park, J.A., Joe, Y.A., Kim, T.G. and Hong, Y.K. (2006) Potentiation of antiglioma effect with combined temozolomide and interferon-beta. *Oncol. Rep.* **16**, 1253–1260

11 Buttmann, M., Berberich-Siebelt, F., Serfling, E. and Rieckmann, P. (2007) Interferon-β is a potent inducer of interferon regulatory factor-1/2-dependent IP-10/CXCL10 expression in primary human endothelial cells. *J. Vasc. Res.* **44**, 51–60, https://doi.org/10.1159/000097977

12 Hogan, N.T., Whalen, M.B., Stolze, L.K., Hadeli, N.K., Lam, M.T., Springstead, J.R. et al. (2017) Transcriptional networks specifying homeostatic and inflammatory programs of gene expression in human aortic endothelial cells. *Elife* **6**, e22536, https://doi.org/10.7554/eLife.22536

13 Rettino, A. and Clarke, N.M. (2013) Genome-wide identification of IRF1 binding sites reveals extensive occupancy at cell death associated genes. *J. Carcinogenesis Mutagenesis* **S6**, 009, https://doi.org/10.4172/2157-2518.S6-009

14 Huang, H., Rose, J.L. and Hoyt, D.G. (2004) p38 Mitogen-activated protein kinase mediates synergistic induction of inducible nitric-oxide synthase by lipopolysaccharide and interferon-γ through signal transducer and activator of transcription 1 Ser727 phosphorylation in murine aortic endothelial cells. *Mol. Pharmacol.* **66**, 302–311, https://doi.org/10.1124/mol.66.2.302

15 Wu, J., Li, X., Huang, L., Jiang, S., Tu, F., Zhang, X. et al. (2015) HSPA12B inhibits lipopolysaccharide-induced inflammatory response in human umbilical vein endothelial cells. *J. Cell. Mol. Med.* **19**, 544–554, https://doi.org/10.1111/jcmm.12464

16 Su, V.Y., Chiou, S.H., Lin, C.S., Mo, M.H. and Yang, K.Y. (2019) Induced pluripotent stem cells attenuate endothelial leakage in acute lung injury via tissue inhibitor of metalloproteinases-1 to reduce focal adhesion kinase activity. *Stem Cells* **37**, 1516–1527, https://doi.org/10.1002/stem.3093

17 Payne, S., De Val, S. and Neal, A. (2018) Endothelial-specific cre mouse models: is your cre credibile? *Arterioscler. Thromb. Vasc. Biol.* **38**, 2550–2561, https://doi.org/10.1161/ATVBAHA.118.309669
18 Xu, M., Cao, F.L., Zhang, Y.F., Shan, L., Jiang, X.L., An, X.J. et al. (2015) Tanshinone IIA therapeutically reduces LPS-induced acute lung injury by inhibiting inflammation and apoptosis in mice. *Acta Pharmacol. Sin.* **36**, 179–187, https://doi.org/10.1038/aps.2014.112
19 Lin, Z.S., Ku, C.F., Guan, Y.F., Xiao, H.T., Shi, X.K., Wang, H.Q. et al. (2016) Dihydro-resveratrol ameliorates lung injury in rats with cerulein-induced acute pancreatitis. *Phytotherapy Res.: PTR* **30**, 663–670, https://doi.org/10.1002/ptr.5576
20 Putz, E.M., Gotthardt, D., Hoermann, G., Csiszar, A., Wirth, S., Berger, A. et al. (2013) CDK8-mediated STAT1-S727 phosphorylation restrains NK cell cytotoxicity and tumor surveillance. *Cell Rep.* **4**, 437–444, https://doi.org/10.1016/j.celrep.2013.07.012
21 Gory, S., Vernet, M., Laurent, M., Dejana, E., Dalmon, J. and Huber, P. (1999) The vascular endothelial-cadherin promoter directs endothelial-specific expression in transgenic mice. *Blood* **93**, 184–192, https://doi.org/10.1182/blood.V93.1.184
22 Ma, H.T., On, K.F., Tsang, Y.H. and Poon, R.Y. (2007) An inducible system for expression and validation of the specificity of short hairpin RNA in mammalian cells. *Nucleic Acids Res.* **35**, e22, https://doi.org/10.1093/nar/gkl1109
23 Kreft, L., Soete, A., Hulpiau, P., Botzki, A., Saeys, Y. and De Bleser, P. (2017) ConTra v3: a tool to identify transcription factor binding sites across species, update 2017. *Nucleic Acids Res.* **45**, W490–W494, https://doi.org/10.1093/nar/gkx376
24 Thomson, S.J., Goh, F.G., Banks, H., Krausgruber, T., Kotenko, S.V., Foxwell, B.M. et al. (2009) The role of transposable elements in the regulation of IFN-λ1 gene expression. *Proc. Natl. Acad. Sci.* **106**, 11564–11569, https://doi.org/10.1073/pnas.0904477106
25 Piaszyk-Borychowska, A., Széles, L., Csermely, A., Chiang, H.-C., Wesoly, J., Lee, C.-K. et al. (2019) Signal integration of IFN-I and IFN-II with TLR4 involves sequential recruitment of STAT1-complexes and NFκB to enhance pro-inflammatory transcription. *Front. Immunol.* **10**, 1253, https://doi.org/10.3389/fimmu.2019.01253
26 Huang, W., Rha, G.B., Han, M.J., Eum, S.Y., András, I.E., Zhong, Y. et al. (2008) PPARalpha and PPARgamma effectively protect against HIV-induced inflammatory responses in brain endothelial cells. *J. Neurochem.* **107**, 497–509, https://doi.org/10.1111/j.1471-4159.2008.05626.x
27 Yamauchi, S., Takeuchi, K., Chihara, K., Honjoh, C., Kato, Y., Yoshiki, H. et al. (2016) STAT1 is essential for the inhibition of hepatitis C virus replication by interferon-λ but not by interferon-α. *Sci. Rep.* **6**, 1–11, https://doi.org/10.1038/srep38336
28 de Morais Ribeiro, L.N., Couto, V.M., Fraceto, L.F. and De Paula, E. (2018) Use of nanoparticle concentration as a tool to understand the structural properties of colloids. *Sci. Rep.* **8**, 1–8
29 Johnsen, K.B., Bak, M., Melander, F., Thomsen, M.S., Burkhart, A., Kempen, P.J. et al. (2019) Modulating the antibody density changes the uptake and transport at the blood-brain barrier of both transferrin receptor-targeted gold nanoparticles and liposomal cargo. *J. Control. Release* **295**, 237–249, https://doi.org/10.1016/j.jconrel.2019.01.005
30 Cheng, K.T., Xiong, S., Ye, Z., Hong, Z., Di, A., Tsang, K.M. et al. (2017) Caspase-11–mediated endothelial pyroptosis underlies endotoxemia-induced lung injury. *J. Clin. Invest.* **127**, 4124–4135, https://doi.org/10.1172/JCI94495
31 Zhou, M.-Y., Lo, S.K., Bergenfeldt, M., Tiruppathi, C., Jaffe, A., Xu, N. et al. (1998) In vivo expression of neutrophil inhibitory factor via gene transfer prevents lipopolysaccharide-induced lung neutrophil infiltration and injury by a beta2 integrin-dependent mechanism. *J. Clin. Invest.* **101**, 2427–2437, https://doi.org/10.1172/JCI407
32 Miyawaki-Shimizu, K., Predescu, D., Shimizu, J., Broman, M., Predescu, S. and Malik, A.B. (2006) siRNA-induced caveolin-1 knockdown in mice increases lung vascular permeability via the junctional pathway. *Am. J. Physiol.-Lung Cell. Mol. Physiol.* **290**, L405–L413, https://doi.org/10.1152/ajplung.00292.2005
33 McColm, J.R., Geisen, P., Peterson, L.J. and Hartnett, M.E. (2006) Exogenous leukemia inhibitory factor (LIF) attenuates retinal vascularization reducing cell proliferation not apoptosis. *Exp. Eye Res.* **83**, 438–446, https://doi.org/10.1016/j.exer.2006.01.027
34 Michalska, A., Blaszczyk, K., Wesoly, J. and Bluyssen, H.A. (2018) A positive feedback amplifier circuit that regulates interferon (IFN)-stimulated gene expression and controls type I and type II IFN responses. *Front. Immunol.* **9**, 1135, https://doi.org/10.3389/fimmu.2018.01135
35 Crapo, J.D., Barry, B.E., Gehr, P., Bachofen, M. and Weibel, E.R. (1982) Cell number and cell characteristics of the normal human lung. *Am. Rev. Respir. Dis.* **126**, 332–337
36 Jambusaria, A., Klomp, J., Hong, Z., Rafii, S., Dai, Y., Malik, A.B. et al. (2018) A computational approach to identify cellular heterogeneity and tissue-specific gene regulatory networks. *BMC Bioinform.* **19**, 217, https://doi.org/10.1186/s12859-018-2190-6
37 Peng, K., Fan, X., Li, Q., Wang, Y., Chen, X., Xiao, P. et al. (2020) IRF-1 mediates the suppressive effects of mTOR inhibition on arterial endothelium. *J. Mol. Cell Cardiol.* **140**, 30–41, https://doi.org/10.1016/j.yjmcc.2020.02.006
38 Lee, J.H., Chun, T., Park, S.-Y. and Rho, S.B. (2008) Interferon regulatory factor-1 (IRF-1) regulates VEGF-induced angiogenesis in HUVECs. *Biochim. Biophys. Acta (BBA)- Mol. Cell Res.* **1783**, 1654–1662, https://doi.org/10.1016/j.bbamcr.2008.04.006
39 Negishi, H., Taniguchi, T. and Yanai, H. (2018) The interferon (IFN) class of cytokines and the IFN regulatory factor (IRF) transcription factor family. *Cold Spring Harbor Perspect. Biol.* **10**, a028423, https://doi.org/10.1101/cshperspect.a028423
40 Abe, J.-i. (2016) Multiple functions of protein inhibitor of activated STAT1 in regulating endothelial cell proliferation and inflammation. *Am. Heart Assoc.*, https://doi.org/10.1161/ATVBAHA.116.308131
41 Zhu, L., Wang, F., Yang, H., Zhang, J. and Chen, S. (2020) Low shear stress damages endothelial function through STAT1 in endothelial cells (ECs). *J. Physiol. Biochem.* **76** (1), 147–57, https://doi.org/10.1007/s13105-020-00729-1
42 Liu, Y., Yu, M. and Jiang, D. (2019) Downregulation of STAT1 induces the differentiation of neural stem cells through JNK pathway. *Tissue Cell.* **61**, 61–66, https://doi.org/10.1016/j.tice.2019.09.004
43 Twohig, J.P., Figueras, A.C., Andrews, R., Wiede, F., Cossins, B.C., Soria, A.D. et al. (2019) Activation of naïve CD4+ T cells re-tunes STAT1 signaling to deliver unique cytokine responses in memory CD4+ T cells. *Nat. Immunol.* **20**, 458–470, https://doi.org/10.1038/s41590-019-0350-0
44 Qin, S., Zhang, Y., Zhang, J., Tian, F., Sun, L., He, X. et al. (2020) SPRY4 regulates trophoblast proliferation and apoptosis via regulating IFN-γ-induced STAT1 expression and activation in recurrent miscarriage. *Am. J. Reprod. Immunol.* **83**, e13234, https://doi.org/10.1111/aji.13234